Thermalization in simple metals: Role of electron-phonon and phonon-phonon scattering

Shota Ono*

Department of Electrical, Electronic and Computer Engineering, Gifu University, Gifu 501-1193, Japan

(Received 6 November 2017; revised manuscript received 25 January 2018; published 20 February 2018)

We study the electron and phonon thermalization in simple metals excited by a laser pulse. The thermalization is investigated numerically by solving the Boltzmann equation taking into account the relevant scattering mechanism: electron-electron, electron-phonon (e-ph), phonon-electron (ph-e), and phonon-phonon (ph-ph) scattering. In the initial stage of the relaxation, most of the excitation energy is transferred from the electrons to phonons through the e-ph scattering. This creates hot high-frequency phonons due to the ph-e scattering, followed by an energy redistribution between phonon subsystems through the ph-ph scattering. This yields an overshoot of the total longitudinal-acoustic phonon energy at a time, across which a crossover occurs from a nonequilibrium state, where the e-ph and ph-e scattering frequently occur, to a state, where the ph-ph scattering occurs to reach a thermal equilibrium. This picture is quite different from the scenario of the well-known two-temperature model (2TM). The behavior of the relaxation dynamics is compared with those calculated by several models, including the 2TM, the four-temperature model, and nonequilibrium electron or phonon models. The relationship between the relaxation time and the initial distribution function is also discussed.

DOI: 10.1103/PhysRevB.97.054310

I. INTRODUCTION

Notwithstanding the fundamental interest in ultrafast dynamics of elementary excitations in solids excited by femtosecond laser pulses the thermalization even in simple metals is not well understood. The aim of this paper is to develop a theory for the thermalization of metals beyond the well-known two-temperature model (2TM), that is, beyond the quasiequilibrium approximation.

The thermalization in metals after a pump pulse irradiation is governed by the electron-electron (e-e), electron-phonon (e-ph), phonon-electron (ph-e), and phonon-phonon (ph-ph) scattering. The energy transfer between electrons and phonons through the e-ph and ph-e scattering has been theoretically studied by Kaganov *et al.* [1], motivated by the electron transport experiment, where a deviation from the Ohm's law was observed in metals. Given that the e-e and ph-ph scattering keep the electron and phonon distributions equal to quasiequilibrium distributions, the energy relaxation can be described by the time evolution of the electron and phonon temperatures. Based on this picture, Anisimov *et al.* have first applied the 2TM to study the energy relaxation of photoexcited systems [2]. Allen has revealed the relationship between the e-ph coupling function used in the 2TM and the Eliashberg function used in the strong coupling theory of superconductivity [3], which has provided how to interpret time-resolved experiments [4–7] and has been a basis for studying the thermalization of condensed matters theoretically [8–10].

However, it has been questionable whether the assumption behind the 2TM is really valid or not. In fact, both the experimental works using time-resolved photoemission spectroscopy [11–14] and the theoretical works based on the Boltzmann equation (BOE) considering the e-e and e-ph scattering [12,15–19] have revealed the breakdown of the 2TM. Furthermore, recent studies have pointed out the importance of the ph-ph scattering for better understanding the thermalization in metals [20–23], semiconductors [24], and Dirac semimetals [25]. Note also that several attempts have been made to extract the e-ph coupling constant from experimental data [26–28] by exploiting the nonequilibrium theory developed in Ref. [16]. In addition, thermalization in microscopic models based on a Holstein-type Hamiltonian has been recently investigated [29–31]. A picture for the thermalization in solids should now be reconsidered without using the quasiequilibrium approximation.

In this paper, we investigate the electron and phonon thermalization in simple metals by solving the BOE taking into account the e-e, e-ph, ph-e, and ph-ph scattering. Through the e-ph scattering, most of the electron energy is transferred into longitudinal acoustic (LA) phonons in the initial stage of the relaxation. Simultaneously, the LA phonon decays into transverse acoustic (TA) phonons via the ph-ph scattering. This yields an overshoot of the total LA phonon energy at a time. Such an overshoot is an indicator for a crossover from a nonequilibrium state, where the e-ph and ph-e scattering frequently occur, to a state, where the ph-ph scattering occurs to reach a thermal equilibrium. Throughout the energy relaxation, the effect of the e-e scattering can be negligible. The thermalization scenario demonstrated is quite different from that of the 2TM [3]. A comparative study using several models shows that the energy relaxation of quasiequilibrium states is faster than that of nonequilibrium states. This implies that an application of the 2TM to time-resolved experiments would lead to an underestimation of the e-ph coupling constant of metals, which is consistent with the results in Ref. [20]. It is also shown that the relaxation time strongly depends on the initial electron and phonon distribution functions as well as their initial energies.

*shota_o@gifu-u.ac.jp

The paper is organized as follows. In Sec. II A, the e-e, e-ph, and ph-ph interaction Hamiltonians are formulated. The matrix elements derived are used for describing the multiparticle scattering events. In Sec. II B, the BOE for the electron and phonon is derived. For later use, several models for the energy relaxation of solids are provided. In Sec. III A, a picture for the thermalization is presented by investigating the time evolution of the excess energy, the energy transfer rate, and the distribution functions for electron and phonon. In Sec. III B, the behavior of relaxation dynamics in the nonequilibrium electron-phonon model is compared with those in other models. The relationship between the relaxation time and the initial distribution function is also discussed. The paper is summarized in Sec. IV.

II. THEORY

We consider the nonequilibrium electron-phonon dynamics in simple metals excited by a laser pulse. The low energy excitation of the electron and the phonon is described by the jellium model and the continuum elasticity model, respectively. The ultrafast dynamics of those elementary particles is regulated by the BOE with the e-e, e-ph, ph-e, and ph-ph collision integrals. Thus, we first formulate the interaction Hamiltonian necessary to describe the scattering processes.

A. Hamiltonian

The total Hamiltonian is written as

$$\mathcal{H} = \mathcal{H}_{\rm e} + \mathcal{H}_{\rm p} + \mathcal{H}_{\rm ep}, \tag{1}$$

where $\mathcal{H}_{\rm e}$, $\mathcal{H}_{\rm p}$, and $\mathcal{H}_{\rm ep}$ denote the electron, the phonon, and the e-ph interaction Hamiltonian, respectively. The former two Hamiltonians include the e-e and ph-ph interaction part, respectively. The expression for each Hamiltonian is given below.

1. Electrons

In a simple metal, the valence electron can be treated as a free electron in the zeroth-order approximation [32]. Since the electrons interact with each other via the Coulomb interaction forces, the electron Hamiltonian is written as [33]

$$\mathcal{H}_{\rm e} = \sum_{\sigma}\int d\boldsymbol{r}\,\psi^{\dagger}_{\sigma}(\boldsymbol{r})\left(-\frac{\hbar^2}{2m}\nabla^2\right)\psi_{\sigma}(\boldsymbol{r}) + \frac{1}{2}\sum_{\sigma,\sigma'}\int d\boldsymbol{r}\int d\boldsymbol{r}'\,\psi^{\dagger}_{\sigma}(\boldsymbol{r})\psi^{\dagger}_{\sigma'}(\boldsymbol{r}')V(|\boldsymbol{x}|)\psi_{\sigma'}(\boldsymbol{r}')\psi_{\sigma}(\boldsymbol{r}), \tag{2}$$

where $\hbar$ is the Planck constant, and m is the electron mass. The first and the second terms are the kinetic and the e-e interaction energies, respectively. $\psi_{\sigma}(\boldsymbol{r})$ is the field operator and is expanded by the plane waves

$$\psi_{\sigma}(\boldsymbol{r}) = \sum_{\boldsymbol{k}} a_{\boldsymbol{k}\sigma}\frac{e^{i\boldsymbol{k}\cdot\boldsymbol{r}}}{\sqrt{\Omega}} \tag{3}$$

with the electron position $\boldsymbol{r}$, the wave vector $\boldsymbol{k}$, the spin σ, and the crystal volume Ω. $a_{\boldsymbol{k}\sigma}$ ($a^{\dagger}_{\boldsymbol{k}\sigma}$) is the destruction (creation) operator of the electron with $\boldsymbol{k}$ and σ. $V(|\boldsymbol{x}|)$ with $\boldsymbol{x} = \boldsymbol{r} - \boldsymbol{r}'$ is the screened Coulomb potential energy given as

$$V(|\boldsymbol{x}|) = \frac{e^2}{4\pi\epsilon_0}\frac{e^{-q_{\rm TF}|\boldsymbol{x}|}}{|\boldsymbol{x}|} \tag{4}$$

with the electron charge e and the dielectric constant of vacuum ϵ_0. $q_{\rm TF}$ is the Thomas-Fermi wave number given by

$$q_{\rm TF}a_0 = \left(\frac{12}{\pi}\right)^{1/3}\frac{1}{\sqrt{r_s}} \tag{5}$$

with the dimensionless Wigner-Seitz radius r_s and the Bohr radius $a_0 = 4\pi\varepsilon_0\hbar^2/(me^2)$. Using the Fourier transformation, Eq. (2) is expressed as

$$\mathcal{H}_{\rm e} = \sum_{\boldsymbol{k}\sigma}\varepsilon_{\boldsymbol{k}}a^{\dagger}_{\boldsymbol{k}\sigma}a_{\boldsymbol{k}\sigma} + \frac{1}{2}\sum_{\boldsymbol{k}_1\sigma_1}\sum_{\boldsymbol{k}_2\sigma_2}\sum_{\boldsymbol{q}}\tilde{V}(\boldsymbol{q})a^{\dagger}_{\boldsymbol{k}_1+\boldsymbol{q}\sigma_1}a^{\dagger}_{\boldsymbol{k}_2-\boldsymbol{q}\sigma_2}a_{\boldsymbol{k}_2\sigma_2}a_{\boldsymbol{k}_1\sigma_1}, \tag{6}$$

where $\varepsilon_{\boldsymbol{k}} = \hbar^2k^2/(2m)$ is the free electron energy and $\tilde{V}(\boldsymbol{q})$ is the Fourier component of the screened Coulomb potential

$$\tilde{V}(\boldsymbol{q}) = \frac{1}{\Omega}\frac{e^2}{\epsilon_0\left(q^2 + q^2_{\rm TF}\right)}, \tag{7}$$

which is independent of the electron spin.

2. Phonons

The lattice dynamics in an atomistic system can be considered as an elastic wave propagation in a continuum medium within a long wavelength limit [32,34]. The Hamiltonian for the latter is given by

$$\mathcal{H}_{\rm p} = \frac{1}{2\rho_{\rm i}}\sum_{i}\int p^{*}_{i}(\boldsymbol{r})p_i(\boldsymbol{r})d\boldsymbol{r} + \frac{1}{2!}\sum_{ijkl}\int d\boldsymbol{r}\,C_{ijkl}\eta_{ij}(\boldsymbol{r})\eta_{kl}(\boldsymbol{r}) + \frac{1}{3!}\sum_{ijklmn}\int d\boldsymbol{r}\,C_{ijklmn}\eta_{ij}(\boldsymbol{r})\eta_{kl}(\boldsymbol{r})\eta_{mn}(\boldsymbol{r}), \tag{8}$$

where C_{ijkl} (C_{ijklmn}) is the forth-rank (six-rank) tensor and serves as the second-order (third-order) elastic constants with $i,j,k,l,m,n = 1,2,3$. $\rho_{\rm i}$ is the ion mass density given by $\rho_{\rm i} = M_{\rm i}N_{\rm i}/\Omega$ with the ion mass $M_{\rm i}$ and the number of the ions $N_{\rm i}$ in a volume Ω. The strain tensor is defined as [35,36]

$$\eta_{ij}(\boldsymbol{r}) = \frac{1}{2}\left(\frac{\partial u_i}{\partial x_j} + \frac{\partial u_j}{\partial x_i} + \sum_{k}\frac{\partial u_k}{\partial x_i}\frac{\partial u_k}{\partial x_j}\right). \tag{9}$$

Within the isotropic approximation, the forth-rank tensor is given by

$$C_{ijkl} = \lambda_{\rm L}\delta_{ij}\delta_{kl} + \mu_{\rm L}(\delta_{ik}\delta_{jl} + \delta_{il}\delta_{jk}), \tag{10}$$

where $\lambda_{\rm L}$ and $\mu_{\rm L}$ are Lamé constants, while the six-rank tensor is given as

$$C_{ijklmn} = E_1\delta_{ij}\delta_{kl}\delta_{mn} + E_2[\delta_{ij}(\delta_{km}\delta_{ln} + \delta_{kn}\delta_{lm}) + \delta_{kl}(\delta_{im}\delta_{jn} + \delta_{in}\delta_{jm})$$

$$+\delta_{mn}(\delta_{ik}\delta_{jl}+\delta_{il}\delta_{jk})]$$
$$+E_3[\delta_{ik}(\delta_{jm}\delta_{ln}+\delta_{jn}\delta_{lm})+\delta_{il}(\delta_{jm}\delta_{kn}+\delta_{jn}\delta_{km})$$
$$+\delta_{im}(\delta_{jk}\delta_{ln}+\delta_{jl}\delta_{kn})+\delta_{in}(\delta_{jk}\delta_{lm}+\delta_{jl}\delta_{km})], \tag{11}$$

where E_1, E_2, and E_3 are the third-order elastic constants. The displacement vector is written as

$$u_i(\boldsymbol{r})=\sum_{\boldsymbol{Q},\gamma}\sqrt{\frac{\hbar}{2\rho_{\rm i}\Omega\omega_\gamma(\boldsymbol{Q})}}(b_{\boldsymbol{Q}\gamma}+b^\dagger_{-\boldsymbol{Q}\gamma})\times e_i(\boldsymbol{Q},\gamma)e^{i\boldsymbol{Q}\cdot\boldsymbol{r}}, \tag{12}$$

where $b_{\boldsymbol{Q}\gamma}$ and $b^\dagger_{\boldsymbol{Q}\gamma}$ are the destruction and creation operators for the phonon with the wave vector $\boldsymbol{Q}=(Q_1,Q_2,Q_3)$ and the polarization $\gamma=$ LA, TA1, and TA2. $e_i(\boldsymbol{Q},\gamma)$ is the ith component of the polarization vector $\boldsymbol{e}(\boldsymbol{Q},\gamma)$. The momentum operator in Eq. (8) is given by

$$p_i(\boldsymbol{r})=-i\sum_{\boldsymbol{Q},\gamma}\sqrt{\frac{\hbar\rho_{\rm i}\omega_\gamma(\boldsymbol{Q})}{2\Omega}}(b_{\boldsymbol{Q}\gamma}-b^\dagger_{-\boldsymbol{Q}\gamma})\times e_i(\boldsymbol{Q},\gamma)e^{i\boldsymbol{Q}\cdot\boldsymbol{r}}. \tag{13}$$

Using the orthonormality of the polarization vectors for a given $\boldsymbol{Q}$,

$$\boldsymbol{e}^*(\boldsymbol{Q},\gamma')\cdot\boldsymbol{e}(\boldsymbol{Q},\gamma)=\delta_{\gamma,\gamma'}, \tag{14}$$

and the elastic wave equation

$$\rho_{\rm i}\omega^2_\gamma(\boldsymbol{Q})e_i(\boldsymbol{Q},\gamma)=\sum_k\left(\sum_{jl}C_{ijkl}Q_jQ_l\right)e_k(\boldsymbol{Q},\gamma), \tag{15}$$

the unperturbed phonon Hamiltonian, that is, the sum of the first and second terms in Eq. (8), is given by

$$\mathcal{H}^0_p=\sum_{\boldsymbol{Q}\gamma}\hbar\omega_\gamma(\boldsymbol{Q})\left(b^\dagger_{\boldsymbol{Q}\gamma}b_{\boldsymbol{Q}\gamma}+\frac{1}{2}\right). \tag{16}$$

The frequencies of the three phonon branches are given by

$$\omega_{\rm LA}(\boldsymbol{Q})=\sqrt{\frac{\lambda_{\rm L}+2\mu_{\rm L}}{\rho_{\rm i}}}|\boldsymbol{Q}|\equiv v_{\rm LA}|\boldsymbol{Q}|,$$
$$\omega_{\rm TA1}(\boldsymbol{Q})=\omega_{\rm TA2}(\boldsymbol{Q})=\sqrt{\frac{\mu_{\rm L}}{\rho_{\rm i}}}|\boldsymbol{Q}|\equiv v_{\rm TA}|\boldsymbol{Q}|, \tag{17}$$

where $v_{\rm LA}$ and $v_{\rm TA}$ are the phonon velocities. The Debye frequency $\Omega_{\gamma,\rm D}$ for the polarization γ is determined by the normalization condition $N_{\rm i}=\int_0^{\Omega_{\gamma,\rm D}}\mathcal{D}_\gamma(\omega)d\omega$, where $\mathcal{D}_\gamma(\omega)$ is the density of states (DOS) for phonons, resulting in $\Omega_{\gamma,\rm D}=v_\gamma(6\pi^2N_{\rm i}/\Omega)^{1/3}$.

The time evolution of the phonon population is governed by the three-phonon process. Substituting Eq. (12) into Eq. (8) and defining

$$\tilde{C}_{ijklmn}=C_{ijlkmn}$$
$$+\lambda_{\rm L}(\delta_{ij}\delta_{km}\delta_{ln}+\delta_{im}\delta_{jn}\delta_{kl}+\delta_{ik}\delta_{jl}\delta_{mn})$$
$$+\mu_{\rm L}(\delta_{ik}\delta_{jm}\delta_{ln}+\delta_{ik}\delta_{jn}\delta_{lm}+\delta_{il}\delta_{jn}\delta_{km}$$
$$+\delta_{im}\delta_{jk}\delta_{ln}+\delta_{im}\delta_{jl}\delta_{kn}+\delta_{in}\delta_{jl}\delta_{km}), \tag{18}$$

one obtains the perturbed Hamiltonian

$$\mathcal{H}'_p=\frac{1}{6}\sum_{\boldsymbol{Q},\boldsymbol{Q}',\boldsymbol{Q}''}\sum_{\gamma,\gamma',\gamma'}A^{\gamma,\gamma',\gamma''}_{\boldsymbol{Q},\boldsymbol{Q}',\boldsymbol{Q}''}\delta_{\boldsymbol{Q}+\boldsymbol{Q}'+\boldsymbol{Q}'',0}$$
$$\times B_{\boldsymbol{Q}\gamma}B_{\boldsymbol{Q}'\gamma'}B_{\boldsymbol{Q}''\gamma''}, \tag{19}$$

where $B_{\boldsymbol{Q}\gamma}=b_{\boldsymbol{Q}\gamma}+b^\dagger_{-\boldsymbol{Q}\gamma}$ and the three-phonon matrix elements $A^{\gamma,\gamma',\gamma'}_{\boldsymbol{Q},\boldsymbol{Q}',\boldsymbol{Q}''}$ that is explicitly given as [37]

$$A^{\gamma,\gamma',\gamma''}_{\boldsymbol{Q},\boldsymbol{Q}',\boldsymbol{Q}''}=\frac{-i}{\sqrt{\Omega}}\left(\frac{\hbar}{2\rho_{\rm i}}\right)^{3/2}\frac{A_{\rm ph}}{\sqrt{\omega_\gamma(\boldsymbol{Q})\omega_{\gamma'}(\boldsymbol{Q}')\omega_{\gamma''}(\boldsymbol{Q}'')}} \tag{20}$$

with

$$A_{\rm ph}=E_1(\boldsymbol{e}\cdot\boldsymbol{Q})(\boldsymbol{e}'\cdot\boldsymbol{Q}')(\boldsymbol{e}''\cdot\boldsymbol{Q}'')$$
$$+E_2(\boldsymbol{e}\cdot\boldsymbol{Q})[(\boldsymbol{e}'\cdot\boldsymbol{e}'')(\boldsymbol{Q}'\cdot\boldsymbol{Q}'')+(\boldsymbol{e}'\cdot\boldsymbol{Q}'')(\boldsymbol{e}''\cdot\boldsymbol{Q}')]$$
$$+E_2(\boldsymbol{e}'\cdot\boldsymbol{Q}')[(\boldsymbol{e}\cdot\boldsymbol{e}'')(\boldsymbol{Q}\cdot\boldsymbol{Q}'')+(\boldsymbol{e}\cdot\boldsymbol{Q}'')(\boldsymbol{e}''\cdot\boldsymbol{Q})]$$
$$+E_2(\boldsymbol{e}''\cdot\boldsymbol{Q}'')[(\boldsymbol{e}\cdot\boldsymbol{e}')(\boldsymbol{Q}\cdot\boldsymbol{Q}')+(\boldsymbol{e}\cdot\boldsymbol{Q}')(\boldsymbol{e}'\cdot\boldsymbol{Q})]$$
$$+E_3(\boldsymbol{e}\cdot\boldsymbol{e}')[(\boldsymbol{e}''\cdot\boldsymbol{Q})(\boldsymbol{Q}'\cdot\boldsymbol{Q}'')+(\boldsymbol{Q}\cdot\boldsymbol{Q}'')(\boldsymbol{e}''\cdot\boldsymbol{Q}')]$$
$$+E_3(\boldsymbol{e}\cdot\boldsymbol{Q}')[(\boldsymbol{e}''\cdot\boldsymbol{Q})(\boldsymbol{e}'\cdot\boldsymbol{Q}'')+(\boldsymbol{Q}\cdot\boldsymbol{Q}'')(\boldsymbol{e}'\cdot\boldsymbol{e}'')]$$
$$+E_3(\boldsymbol{e}\cdot\boldsymbol{e}'')[(\boldsymbol{e}'\cdot\boldsymbol{Q})(\boldsymbol{Q}'\cdot\boldsymbol{Q}'')+(\boldsymbol{Q}\cdot\boldsymbol{Q}')(\boldsymbol{e}'\cdot\boldsymbol{Q}'')]$$
$$+E_3(\boldsymbol{e}\cdot\boldsymbol{Q}'')[(\boldsymbol{e}'\cdot\boldsymbol{Q})(\boldsymbol{e}''\cdot\boldsymbol{Q}')+(\boldsymbol{Q}\cdot\boldsymbol{Q}')(\boldsymbol{e}'\cdot\boldsymbol{e}'')]$$
$$+\lambda_{\rm L}[(\boldsymbol{e}\cdot\boldsymbol{Q})(\boldsymbol{e}'\cdot\boldsymbol{e}'')(\boldsymbol{Q}'\cdot\boldsymbol{Q}'')$$
$$+(\boldsymbol{e}\cdot\boldsymbol{e}'')(\boldsymbol{Q}\cdot\boldsymbol{Q}'')(\boldsymbol{e}'\cdot\boldsymbol{Q}')+(\boldsymbol{e}\cdot\boldsymbol{e}')(\boldsymbol{Q}\cdot\boldsymbol{Q}')(\boldsymbol{e}''\cdot\boldsymbol{Q}'')]$$
$$+\mu_{\rm L}[(\boldsymbol{e}\cdot\boldsymbol{e}')(\boldsymbol{Q}\cdot\boldsymbol{e}'')(\boldsymbol{Q}'\cdot\boldsymbol{Q}'')$$
$$+(\boldsymbol{e}\cdot\boldsymbol{e}')(\boldsymbol{Q}\cdot\boldsymbol{Q}'')(\boldsymbol{Q}'\cdot\boldsymbol{e}'')+(\boldsymbol{e}\cdot\boldsymbol{Q}')(\boldsymbol{Q}\cdot\boldsymbol{Q}'')(\boldsymbol{e}'\cdot\boldsymbol{e}'')$$
$$+(\boldsymbol{e}\cdot\boldsymbol{e}'')(\boldsymbol{Q}\cdot\boldsymbol{e}')(\boldsymbol{Q}'\cdot\boldsymbol{Q}'')+(\boldsymbol{e}\cdot\boldsymbol{e}'')(\boldsymbol{Q}\cdot\boldsymbol{Q}')(\boldsymbol{e}'\cdot\boldsymbol{Q}'')$$
$$+(\boldsymbol{e}\cdot\boldsymbol{Q}'')(\boldsymbol{Q}\cdot\boldsymbol{Q}')(\boldsymbol{e}'\cdot\boldsymbol{e}'')] \tag{21}$$

with the abbreviation $\boldsymbol{e}=\boldsymbol{e}(\boldsymbol{Q}\gamma)$, $\boldsymbol{e}'=\boldsymbol{e}(\boldsymbol{Q}'\gamma')$, and $\boldsymbol{e}''=\boldsymbol{e}(\boldsymbol{Q}''\gamma'')$. Note that $A_{\rm ph}$ is symmetric under the exchanges $(\boldsymbol{e},\boldsymbol{Q})\leftrightarrow(\boldsymbol{e}',\boldsymbol{Q}')$, $(\boldsymbol{e}',\boldsymbol{Q}')\leftrightarrow(\boldsymbol{e}'',\boldsymbol{Q}'')$, and $(\boldsymbol{e},\boldsymbol{Q})\leftrightarrow(\boldsymbol{e}'',\boldsymbol{Q}'')$.

3. Electron-phonon interaction

The electron-lattice interaction Hamiltonian is expanded into two terms: the static and dynamical lattice potential. The former and the latter contribute to the Bloch electron formation and the energy exchange during the relaxation. The leading term in the latter is the deformation potential interaction [38]. The e-ph interaction Hamiltonian is given by

$$\mathcal{H}_{\rm ep}=\sum_\sigma\int d\boldsymbol{r}\psi^\dagger_\sigma(\boldsymbol{r})(D_0\nabla\cdot\boldsymbol{u})\psi_\sigma(\boldsymbol{r})$$
$$=\sum_{\boldsymbol{k},\sigma}\sum_{\boldsymbol{Q},\gamma}g(\boldsymbol{Q},\gamma)a^\dagger_{\boldsymbol{k}+\boldsymbol{Q}\sigma}a_{\boldsymbol{k}\sigma}B_{\boldsymbol{Q}\gamma}, \tag{22}$$

where D_0 is the deformation potential, which describes the interaction between the electron and LA phonon through the local density fluctuations of continuum medium. Within the free-electron approximation, $D_0=2\varepsilon_F/3$ with ε_F being the Fermi energy. Then, one obtains

$$|g(\boldsymbol{Q},\gamma)|^2=D_0^2\frac{\hbar|\boldsymbol{Q}|}{2\rho_{\rm i}\Omega v_{\rm LA}}\delta_{\gamma,\rm LA}. \tag{23}$$

The matrix elements of the electron-TA phonon interaction is finite when one considers the umklapp processes. To treat it phenomenologically, we introduce the polarization-dependent deformation potential D_γ and assume

$$|g(\boldsymbol{Q},\gamma)|^2 = D_\gamma^2 \frac{\hbar|\boldsymbol{Q}|}{2\rho_{\rm i}\Omega v_\gamma}, \tag{24}$$

where $D_{\rm LA} = D_0$ and $D_{\rm TA} = (v_{\rm TA}/v_{\rm LA})^\beta D_0$. The parameter β is determined to yield a realistic value of the e-ph coupling constant described below.

B. Models

We will formulate five models depending on the approximation level. In the first model given in Sec. II B 1, the presence of the quasiequilibrium states is not assumed, while in the 2TM given in Sec. II B 5 it is assumed *a priori*.

1. NEP model

We first present the nonequilibrium electron and phonon (NEP) model, where the relevant scattering processes are considered. We thus expect that the NEP model would yield a relaxation dynamics quite similar to the ultrafast dynamics observed in time-resolved experiments. The BOE for electron and phonon systems is written as [35]

$$\frac{\partial f_{\boldsymbol{k},\sigma}}{\partial t} = \left(\frac{\partial f}{\partial t}\right)_{\rm e-e} + \left(\frac{\partial f}{\partial t}\right)_{\rm e-ph}, \tag{25}$$

$$\frac{\partial n_{\boldsymbol{Q},\gamma}}{\partial t} = \left(\frac{\partial n}{\partial t}\right)_{\rm ph-e} + \left(\frac{\partial n}{\partial t}\right)_{\rm ph-ph}, \tag{26}$$

where no contribution from the diffusion and external field terms is assumed. $f_{\boldsymbol{k},\sigma}$ denotes the distribution function of the electron state with $(\boldsymbol{k},\sigma)$. $n_{\boldsymbol{Q},\gamma}$ denotes the distribution function of the phonon state with $(\boldsymbol{Q},\gamma)$. The first and second terms in Eq. (25) indicate the e-e and e-ph collision integrals, respectively, while the first and second terms in Eq. (26) indicate the ph-e and ph-ph collision integrals, respectively.

Given no magnetic impurities and weak exchange interaction between electrons in the system, it is reasonable to assume that the electron distribution is independent of the spin coordinate, that is,

$$f_{\boldsymbol{k},\uparrow} = f_{\boldsymbol{k},\downarrow} \equiv f_{\boldsymbol{k}}. \tag{27}$$

The transition probability for the scattering events is formulated within the Fermi's golden rule. Using Eqs. (6), (19), (22), and (24), the e-e, e-ph, ph-e, and ph-ph collision integrals are written as

$$\left(\frac{\partial f}{\partial t}\right)_{\rm e-e} = \sum_{\boldsymbol{k}',\boldsymbol{q}} \frac{2\pi}{\hbar}|\tilde{V}(\boldsymbol{q})|^2\delta(\Delta\varepsilon)[-f_{\boldsymbol{k}}f_{\boldsymbol{k}'}(1-f_{\boldsymbol{k}+\boldsymbol{q}})(1-f_{\boldsymbol{k}'-\boldsymbol{q}}) + (1-f_{\boldsymbol{k}})(1-f_{\boldsymbol{k}'})f_{\boldsymbol{k}+\boldsymbol{q}}f_{\boldsymbol{k}'-\boldsymbol{q}}], \tag{28}$$

$$\left(\frac{\partial f}{\partial t}\right)_{\rm e-ph} = \sum_{\boldsymbol{Q},\gamma} \frac{2\pi}{\hbar}|g(\boldsymbol{Q},\gamma)|^2\{-f_{\boldsymbol{k}}(1-f_{\boldsymbol{k}+\boldsymbol{Q}})[n_{\boldsymbol{Q}}^{(+)}\delta(\varepsilon_{\boldsymbol{k}}-\varepsilon_{\boldsymbol{k}+\boldsymbol{Q}}-\hbar\omega_{\boldsymbol{Q}\gamma}) + n_{\boldsymbol{Q}}\delta(\varepsilon_{\boldsymbol{k}}-\varepsilon_{\boldsymbol{k}+\boldsymbol{Q}}+\hbar\omega_{\boldsymbol{Q}\gamma})]$$
$$+(1-f_{\boldsymbol{k}})f_{\boldsymbol{k}+\boldsymbol{Q}}[n_{\boldsymbol{Q}}^{(+)}\delta(\varepsilon_{\boldsymbol{k}}-\varepsilon_{\boldsymbol{k}+\boldsymbol{Q}}+\hbar\omega_{\boldsymbol{Q}\gamma}) + n_{\boldsymbol{Q}}\delta(\varepsilon_{\boldsymbol{k}}-\varepsilon_{\boldsymbol{k}+\boldsymbol{Q}}-\hbar\omega_{\boldsymbol{Q}\gamma})]\}, \tag{29}$$

$$\left(\frac{\partial n}{\partial t}\right)_{\rm ph-e} = \sum_{\boldsymbol{k}} \frac{4\pi}{\hbar}|g(\boldsymbol{Q},\gamma)|^2 f_{\boldsymbol{k}}(1-f_{\boldsymbol{k}+\boldsymbol{Q}})[-n_{\boldsymbol{Q},\gamma}\delta(\varepsilon_{\boldsymbol{k}}-\varepsilon_{\boldsymbol{k}+\boldsymbol{Q}}+\hbar\omega_{\boldsymbol{Q}\gamma}) + n_{\boldsymbol{Q},\gamma}^{(+)}\delta(\varepsilon_{\boldsymbol{k}}-\varepsilon_{\boldsymbol{k}+\boldsymbol{Q}}-\hbar\omega_{\boldsymbol{Q}\gamma})], \tag{30}$$

$$\left(\frac{\partial n}{\partial t}\right)_{\rm ph-ph} = \sum_{\boldsymbol{Q}'\gamma'}\sum_{\gamma''} \frac{2\pi}{\hbar}\left|A^{\gamma,\gamma',\gamma''}_{\boldsymbol{Q},\boldsymbol{Q}',-(\boldsymbol{Q}+\boldsymbol{Q}')}\right|^2\{\tfrac{1}{2}[n_{\boldsymbol{Q},\gamma}^{(+)}n_{-\boldsymbol{Q}',\gamma'}n_{\boldsymbol{Q}+\boldsymbol{Q}',\gamma''} - n_{\boldsymbol{Q},\gamma}n_{-\boldsymbol{Q}',\gamma'}^{(+)}n_{\boldsymbol{Q}+\boldsymbol{Q}',\gamma''}^{(+)}]$$
$$\times\delta(\hbar\omega_{\boldsymbol{Q},\gamma} - \hbar\omega_{-\boldsymbol{Q}',\gamma'} - \hbar\omega_{\boldsymbol{Q}+\boldsymbol{Q}',\gamma''})$$
$$+[n_{\boldsymbol{Q},\gamma}^{(+)}n_{\boldsymbol{Q}',\gamma'}^{(+)}n_{\boldsymbol{Q}+\boldsymbol{Q}',\gamma''} - n_{\boldsymbol{Q},\gamma}n_{\boldsymbol{Q}',\gamma'}n_{\boldsymbol{Q}+\boldsymbol{Q}',\gamma''}^{(+)}]\delta(\hbar\omega_{\boldsymbol{Q},\gamma} + \hbar\omega_{\boldsymbol{Q}',\gamma'} - \hbar\omega_{\boldsymbol{Q}+\boldsymbol{Q}',\gamma''})\}, \tag{31}$$

where $\Delta\varepsilon = \varepsilon_{\boldsymbol{k}} + \varepsilon_{\boldsymbol{k}'} - \varepsilon_{\boldsymbol{k}+\boldsymbol{q}} - \varepsilon_{\boldsymbol{k}'-\boldsymbol{q}}$ and $n_{\boldsymbol{Q},\gamma}^{(+)} = n_{\boldsymbol{Q},\gamma} + 1$. Equation (28) describes the electron scattering $(\boldsymbol{k},\boldsymbol{k}') \leftrightarrows (\boldsymbol{k}+\boldsymbol{q},\boldsymbol{k}'-\boldsymbol{q})$ governed by the screened Coulomb interaction potential $\tilde{V}(\boldsymbol{q})$ in Eq. (7). Equations (29) and (30) describes the e-ph and ph-e scattering, where the electron with $\boldsymbol{k}$ is scattered into that with $\boldsymbol{k}+\boldsymbol{Q}$ by an absorption of the phonon with $\boldsymbol{Q}$ or an emission of the phonon with $-\boldsymbol{Q}$, and vice versa. The first and second terms in Eq. (31) denote the anharmonic phonon decay and inelastic scattering, respectively, with the total wave vector conserved. For the former process, the phonon mode with $(\boldsymbol{Q},\gamma)$ decays into two phonons of $(\boldsymbol{Q}',\gamma')$ and $(\boldsymbol{Q}-\boldsymbol{Q}',\gamma'')$, while for the latter one, the two phonon modes with $(\boldsymbol{Q},\gamma)$ and $(\boldsymbol{Q}',\gamma')$ are merged into a phonon with $(\boldsymbol{Q}+\boldsymbol{Q}',\gamma'')$. In the derivation of the collision terms, Eqs. (29), (30), and (31), the relations $\omega_{\boldsymbol{Q}\gamma} = \omega_{-\boldsymbol{Q}\gamma}$ and $n_{\boldsymbol{Q},\gamma} = n_{-\boldsymbol{Q},\gamma}$ arising from the inversion symmetry are used.

Note that, for a simple metal, there are no three-phonon processes in which all three phonons belong to the same polarization branches. This is due to the dispersion effect near the zone boundary [35]. In the present study, one can neglect the three-phonon processes, such as LA (TA) $\leftrightarrows$ LA (TA) + LA (TA). Besides, there are no scattering processes in which one TA phonon creates two LA phonons, and vice versa, due to the energy conservation law [35].

When $f_{\boldsymbol{k}}$ is averaged over the electron states having the energy ε, one obtains the distribution function for the electron state with the energy ε [16,18]

$$f(\varepsilon) = \frac{1}{\mathcal{N}(\varepsilon)} \sum_{\boldsymbol{k}} \delta(\varepsilon - \varepsilon_{\boldsymbol{k}}) f_{\boldsymbol{k}}, \tag{32}$$

where $\mathcal{N}(\varepsilon) = \Omega(2m)^{3/2}\sqrt{\varepsilon}/(4\pi^2\hbar^3)$ is the electron DOS per spin. Similarly, the phonon distribution function for the phonon states with the frequency ω is defined as [16,18]

$$n_\gamma(\omega) = \frac{1}{\mathcal{D}_\gamma(\omega)} \sum_{\boldsymbol{Q}} \delta(\omega - \omega_{\boldsymbol{Q}\gamma}) n_{\boldsymbol{Q},\gamma}, \tag{33}$$

where $\mathcal{D}_\gamma(\omega) = \Omega\omega^2/(2\pi^2 v_\gamma^3)\theta_{\rm H}(\Omega_{\gamma,\rm D} - \omega)$ is the phonon DOS for the polarization γ. $\theta_{\rm H}(x)$ is the Heaviside step function: $\theta(x) = 1$ for $x \geqslant 1$ and $\theta(x) = 0$ for $x < 1$. By using Eqs. (32) and (33), the time (t) evolution for the electron and phonon distribution functions are given by, respectively,

$$\begin{aligned}\frac{\partial f(\varepsilon)}{\partial t} = {} & 2\pi \int d\varepsilon' \int d\xi \int d\xi' C_{\rm e-e}(\varepsilon,\varepsilon',\xi,\xi')\delta(\varepsilon+\varepsilon'-\xi-\xi')\{-f(\varepsilon)f(\varepsilon')[1-f(\xi)][1-f(\xi')] \\ & + [1-f(\varepsilon)][1-f(\varepsilon')]f(\xi)f(\xi')\} + 2\pi \sum_\gamma \int d\xi \int d\omega C_{\rm e-ph}(\varepsilon,\xi,\omega,\gamma)\big(\delta(\varepsilon-\xi-\hbar\omega)\{[f(\xi)-f(\varepsilon)]n_\gamma(\omega) \\ & - f(\varepsilon)[1-f(\xi)]\} + \delta(\varepsilon-\xi+\hbar\omega)\{[f(\xi)-f(\varepsilon)]n_\gamma(\omega) + f(\xi)[1-f(\varepsilon)]\}\big)\end{aligned} \tag{34}$$

and

$$\begin{aligned}\frac{\partial n_\gamma(\omega)}{\partial t} = {} & 4\pi \int d\varepsilon \int d\xi C_{\rm ph-e}(\varepsilon,\xi,\omega,\gamma) f(\varepsilon)[1-f(\xi)]\{-n_\gamma(\omega)\delta(\varepsilon-\xi+\hbar\omega) + [n_\gamma(\omega)+1]\delta(\varepsilon-\xi-\hbar\omega)\} \\ & + 2\pi \sum_{\gamma'}\sum_{\gamma''} \int d\omega' \int d\omega'' C_{\rm ph-ph}(\omega,\omega',\omega'',\gamma,\gamma',\gamma'') \\ & \times \big\{\tfrac{1}{2}\big[n_\gamma^{(+)}(\omega) n_{\gamma'}(\omega') n_\gamma''(\omega'') - n_\gamma(\omega) n_{\gamma'}^{(+)}(\omega') n_{\gamma''}^{(+)}(\omega'')\big]\delta(\hbar\omega - \hbar\omega' - \hbar\omega'') \\ & + \big[n_\gamma^{(+)}(\omega) n_{\gamma'}^{(+)}(\omega') n_\gamma''(\omega'') - n_\gamma(\omega) n_{\gamma'}(\omega') n_{\gamma''}^{(+)}(\omega'')\big]\delta(\hbar\omega + \hbar\omega' - \hbar\omega'')\big\}\end{aligned} \tag{35}$$

with γ = LA, TA1, and TA2. We introduced the coupling functions defined as

$$C_{\rm e-e}(\varepsilon,\varepsilon',\xi,\xi') = \frac{1}{\hbar\mathcal{N}(\varepsilon)} \sum_{\boldsymbol{k},\boldsymbol{k}',\boldsymbol{q}} |\tilde{V}(\boldsymbol{q})|^2 \delta(\varepsilon - \varepsilon_{\boldsymbol{k}})\delta(\varepsilon' - \varepsilon_{\boldsymbol{k}'})\delta(\xi - \varepsilon_{\boldsymbol{k}+\boldsymbol{q}})\delta(\xi' - \varepsilon_{\boldsymbol{k}'-\boldsymbol{q}}), \tag{36}$$

$$C_{\rm e-ph}(\varepsilon,\xi,\omega,\gamma) = \frac{1}{\hbar\mathcal{N}(\varepsilon)} \sum_{\boldsymbol{k},\boldsymbol{Q}} |\tilde{g}(\boldsymbol{Q},\gamma)|^2 \delta(\varepsilon - \varepsilon_{\boldsymbol{k}})\delta(\xi - \varepsilon_{\boldsymbol{k}+\boldsymbol{Q}})\delta(\omega - \omega_{\boldsymbol{Q}\gamma}), \tag{37}$$

$$C_{\rm ph-e}(\varepsilon,\xi,\omega,\gamma) = \frac{1}{\hbar\mathcal{D}_\gamma(\omega)} \sum_{\boldsymbol{k},\boldsymbol{Q}} |\tilde{g}(\boldsymbol{Q},\gamma)|^2 \delta(\varepsilon - \varepsilon_{\boldsymbol{k}})\delta(\xi - \varepsilon_{\boldsymbol{k}+\boldsymbol{Q}})\delta(\omega - \omega_{\boldsymbol{Q}\gamma}), \tag{38}$$

$$C_{\rm ph-ph}(\omega,\omega',\omega'',\gamma,\gamma',\gamma'') = \frac{1}{\hbar\mathcal{D}_\gamma(\omega)} \sum_{\boldsymbol{Q},\boldsymbol{Q}'} |\tilde{A}^{\gamma,\gamma',\gamma''}_{\boldsymbol{Q},\boldsymbol{Q}',-(\boldsymbol{Q}+\boldsymbol{Q}')}|^2 \delta(\omega - \omega_{\boldsymbol{Q}\gamma})\delta(\omega' - \omega_{\boldsymbol{Q}'\gamma'})\delta(\omega'' - \omega_{\boldsymbol{Q}+\boldsymbol{Q}'\gamma''}). \tag{39}$$

For an isotropic system, these coupling functions are expressed as follows: The e-e coupling function in Eq. (36),

$$\begin{aligned}C_{\rm e-e}(\varepsilon,\varepsilon';\xi,\xi') = {} & \frac{1}{4\pi^2\varepsilon_F^2}\sqrt{\frac{\varepsilon_F}{\varepsilon}}\frac{\hbar}{ma_0^2}\int_0^\infty ds\left[\frac{1}{s^2+(q_{\rm TF}/k_{\rm F})^2}\right]^2 \\ & \times \theta_{\rm H}[1-h_1(\varepsilon,\xi,s)]\theta_{\rm H}[1+h_1(\varepsilon,\xi,s)] \\ & \times \theta_{\rm H}[1-h_1(\varepsilon',\xi',s)]\theta_{\rm H}[1+h_1(\varepsilon',\xi',s)],\end{aligned} \tag{40}$$

with the Fermi wavenumber $k_{\rm F}$, the e-ph coupling function in Eq. (37),

$$\begin{aligned}C_{\rm e-ph}(\varepsilon,\xi,\omega,\gamma) = {} & \frac{3Z_{\rm val}}{128}\sqrt{\frac{\varepsilon_F}{\varepsilon}}\left(\frac{D_\gamma}{\varepsilon_F}\right)^2 \frac{(\hbar\omega)^2}{\left(\frac{1}{2}M_i v_\gamma^2\right)\left(\frac{1}{2}m v_\gamma^2\right)} \\ & \times \theta_{\rm H}[1-h_2(\varepsilon,\xi,\omega)]\theta_{\rm H}[1+h_2(\varepsilon,\xi,\omega)],\end{aligned} \tag{41}$$

where $Z_{\rm val}$ is the number of the valence electron, and the ph-e coupling function in Eq. (38),

$$C_{\rm ph-e}(\varepsilon,\xi,\omega,\gamma) = \frac{\mathcal{N}(\varepsilon)}{\mathcal{D}_\gamma(\omega)} C_{\rm e-ph}(\varepsilon,\xi,\omega,\gamma), \tag{42}$$

where the functions h_1 and h_2 in Eqs. (40) and (41) are given by

$$h_1(\varepsilon,\xi,s) = \frac{1}{2s}\sqrt{\frac{\varepsilon_F}{\varepsilon}}\left(\frac{\xi}{\varepsilon_F} - \frac{\varepsilon}{\varepsilon_F} - s^2\right), \tag{43}$$

$$h_2(\varepsilon,\xi,\omega) = \sqrt{\frac{K_\gamma \varepsilon_F^2}{(\hbar\omega)^2\varepsilon}}\left[\frac{\xi}{\varepsilon_F} - \frac{\varepsilon}{\varepsilon_F} - \frac{(\hbar\omega)^2}{4K_\gamma\varepsilon_F}\right] \tag{44}$$

with $K_\gamma = mv_\gamma^2/2$. Note that when $\varepsilon = \xi = \varepsilon_F$, $C_{\mathrm{e-ph}}(\varepsilon,\xi,\omega,\gamma)$ is related to the Eliashberg function for the polarization γ [16,18]

$$C_{\mathrm{e-ph}}(\varepsilon_F,\varepsilon_F,\omega,\gamma) = \alpha^2F(\omega,\gamma) \tag{45}$$

with $\alpha^2F(\omega) = \sum_\gamma \alpha^2F(\omega,\gamma)$. Using this approximation, the e-ph coupling constants are defined by

$$\lambda_\gamma\langle\omega^n\rangle = 2\int_0^{\Omega_{\gamma,\mathrm{D}}} d\omega\alpha^2F(\omega,\gamma)\omega^{n-1} \tag{46}$$

with $\lambda\langle\omega^n\rangle = \sum_\gamma \lambda_\gamma\langle\omega^n\rangle$. When the deviation of the single particle energy from the Fermi energy is not negligible, we use the expression of

$$C_{\mathrm{e-ph}}(\varepsilon,\xi,\omega,\gamma) \simeq \sqrt{\frac{\varepsilon_\mathrm{F}}{\varepsilon}}\alpha^2F(\omega,\gamma), \tag{47}$$

where the factor $\sqrt{\varepsilon_\mathrm{F}/\varepsilon}$ is multiplied [see the expression of Eq. (41)], which will be used in Sec. II B 2.

The ph-ph coupling function satisfies, by definition, the following properties

$$\begin{aligned} &C_{\mathrm{ph-ph}}(\omega,\omega',\omega'',\gamma,\gamma',\gamma'') \\ &= C_{\mathrm{ph-ph}}(\omega,\omega'',\omega',\gamma,\gamma'',\gamma') \\ &= \frac{\mathcal{D}_{\gamma'}(\omega')}{\mathcal{D}_\gamma(\omega)}C_{\mathrm{ph-ph}}(\omega',\omega,\omega'',\gamma',\gamma,\gamma''). \end{aligned} \tag{48}$$

The derivation of a simple expression for the ph-ph coupling function is difficult, so that we evaluate $C_{\mathrm{ph-ph}}$ in Eq. (39) numerically. The details including the derivation of Eqs. (40) and (41), and the numerical implementation of Eq. (39), will be provided in Appendix.

2. NE+3T model

Second, we present a model that consists of the nonequilibrium electrons and the quasiequilibrium phonons characterized by three phonon temperatures (NE+3T model). We assume that the effect of the e-e and ph-ph scattering on the thermalization is negligible in the initial relaxation. Then, Eq. (34) is simplified into

$$\frac{\partial f(\varepsilon)}{\partial t} = 2\pi\sum_\gamma\sum_{s=\pm}\int d\omega\sqrt{\frac{\varepsilon_\mathrm{F}}{\varepsilon}}\alpha^2F(\omega,\gamma)U(\varepsilon,\omega,\gamma,s), \tag{49}$$

where

$$\begin{aligned} U(\varepsilon,\omega,\gamma,s) = {}& [f(\varepsilon+s\hbar\omega) - f(\varepsilon)]n_{\mathrm{BE}}\left(\omega,T_{\mathrm{ph}}^{(\gamma)}\right) \\ &+ sf(\varepsilon)[1 - f(\varepsilon+s\hbar\omega)] \end{aligned} \tag{50}$$

with the Bose-Einstein (BE) function $n_{\mathrm{BE}}(\omega,T_{\mathrm{ph}}^{(\gamma)})$. $T_{\mathrm{ph}}^{(\gamma)}$ is the phonon temperature for the polarization γ. Since the net phonon energy with γ is defined by $E_{\mathrm{ph},\gamma}^{(\mathrm{net})} = \int d\omega\hbar\omega\mathcal{D}_\gamma(\omega)n_{\mathrm{BE}}(\omega,T_{\mathrm{ph}}^{(\gamma)})$, the t evolution of $T_{\mathrm{ph}}^{(\gamma)}$ can be expressed as, by using Eq. (35),

$$\begin{aligned} C_{\mathrm{ph}}^{(\gamma)}\frac{\partial T_{\mathrm{ph}}^{(\gamma)}}{\partial t} = {}& 4\pi\mathcal{N}(\varepsilon_F)\int d\varepsilon\int d\omega\hbar\omega \\ &\times\sqrt{\frac{\varepsilon_\mathrm{F}}{\varepsilon}}\alpha^2F(\omega,\gamma)U(\varepsilon,\omega,\gamma,+), \end{aligned} \tag{51}$$

where $C_{\mathrm{ph}}^{(\gamma)} = \partial E_{\mathrm{ph},\gamma}^{(\mathrm{net})}/\partial T_{\mathrm{ph}}^{(\gamma)}$ is the specific heat of the phonon with γ.

3. NP+1T model

Third, we present a model that consists of the nonequilibrium phonons and the quasiequilibrium electrons (NP+1T model). The net electron energy is $E_\mathrm{e}^{(\mathrm{net})} = 2\int d\varepsilon\varepsilon\mathcal{N}(\varepsilon)f_{\mathrm{FD}}(\varepsilon,T_\mathrm{e})$, where T_e is the electron temperature and f_{FD} is the Fermi-Dirac (FD) function. The t evolution of $E_\mathrm{e}^{(\mathrm{net})}$ is expressed by

$$\frac{\partial E_\mathrm{e}^{(\mathrm{net})}}{\partial t} = -4\pi\mathcal{N}(\varepsilon_F)\sum_\gamma\int d\omega\alpha^2F(\omega,\gamma)(\hbar\omega)^2\nu_\gamma(\omega,T_\mathrm{e}), \tag{52}$$

where

$$\nu_\gamma(\omega,T_\mathrm{e}) = n_{\mathrm{BE}}(\omega,T_\mathrm{e}) - n_\gamma(\omega). \tag{53}$$

In the derivation of Eq. (52), we assumed that the e-ph coupling function is approximated to the Eliashberg function $\alpha^2F(\omega,\gamma)$. Again, the contribution from the e-e and ph-ph scattering are omitted in Eq. (52). Thus, Eq. (52) is a natural extension of Eq. (10) in Ref. [3], since the formula is appropriate for the presence of nonequilibrium phonons. Using the Sommerfeld expansion [32], $E_\mathrm{e}^{(\mathrm{net})}$ is expressed by the t-dependent temperature $T_\mathrm{e}(t)$, that is, $E_\mathrm{e}^{(\mathrm{net})}(t) = 3N_\mathrm{e}\varepsilon_F/5 + \pi^2\mathcal{N}(\varepsilon_F)[k_\mathrm{B}T_\mathrm{e}(t)]^2/3$ with the total number of the electrons N_e. Then, one obtains

$$\frac{\partial T_\mathrm{e}}{\partial t} = -\frac{6}{\pi k_B^2T_\mathrm{e}}\sum_\gamma\int d\omega\alpha^2F(\omega,\gamma)(\hbar\omega)^2\nu_\gamma(\omega,T_\mathrm{e}). \tag{54}$$

Using Eq. (35), the t evolution of $n_\gamma(\omega)$ is simply written as

$$\frac{\partial n_\gamma(\omega)}{\partial t} = \frac{4\pi\mathcal{N}(\varepsilon_F)\hbar\omega}{\mathcal{D}_\gamma(\omega)}\alpha^2F(\omega,\gamma)\nu_\gamma(\omega,T_\mathrm{e}). \tag{55}$$

4. 4TM

To further simplify the model, we assume that the electron and each phonon subset are also quasiequilibrium. We replace $f(\varepsilon)$ in Eq. (51) and $n_\gamma(\omega)$ in Eq. (54) with $f_{\mathrm{FD}}(\varepsilon,T_\mathrm{e})$ and $n_{\mathrm{BE}}(\omega,T_{\mathrm{ph}}^{(\gamma)})$, respectively. Using the high temperature approximation $\hbar\omega/(k_\mathrm{B}T) \ll 1$, that is, $n_{\mathrm{BE}} \simeq k_\mathrm{B}T/(\hbar\omega)$, one obtains the 4TM

$$\begin{aligned} C_\mathrm{e}\frac{\partial T_\mathrm{e}}{\partial t} &= -\sum_\gamma g_\gamma\left(T_\mathrm{e} - T_{\mathrm{ph}}^{(\gamma)}\right), \\ C_{\mathrm{ph}}^{(\gamma)}\frac{\partial T_{\mathrm{ph}}^{(\gamma)}}{\partial t} &= g_\gamma\left(T_\mathrm{e} - T_{\mathrm{ph}}^{(\gamma)}\right), \end{aligned} \tag{56}$$

where C_e is the specific heat of the electron. The coefficient g_γ is written as

$$\frac{g_\gamma}{C_e} = \frac{3\hbar\lambda_\gamma\langle\omega^2\rangle}{\pi k_B T_e}. \tag{57}$$

5. 2TM

In the original derivation of the 2TM by Allen [3], all the phonon temperatures are assumed to be the same. Then, one obtains

$$\begin{aligned} C_e\frac{\partial T_e}{\partial t} &= -G(T_e - T_{ph}),\\ C_{ph}\frac{\partial T_{ph}}{\partial t} &= G(T_e - T_{ph}), \end{aligned} \tag{58}$$

where $G = \sum_\gamma g_\gamma$. The important fact is that the coefficient G in the 2TM contains the e-ph coupling constant $\lambda\langle\omega^2\rangle = \sum_\gamma \lambda_\gamma\langle\omega^2\rangle$. The measurement of T_e as a function of t will make it possible to determine the magnitude of $\lambda\langle\omega^2\rangle$, if many assumptions above, which might be difficult to be satisfied, are correct.

C. Computational details

In the present model, the material properties are described by six parameters which will be provided below. We study the thermalization of aluminum (Al), the most studied simple metal. Thus, we set $r_s = 2.07$ [32]. To determine the elastic constants of the isotropic system from those of a real solid, we minimize X_2 and X_3 defined as [37]

$$\begin{aligned} X_2 &= \sum_{ijkl}(G_{ijkl} - C_{ijkl})^2,\\ X_3 &= \sum_{ijklmn}(G_{ijklmn} - C_{ijklmn})^2, \end{aligned} \tag{59}$$

where G_{ijkl} and G_{ijklmn} are the elastic constants of a realistic system. For cubic crystals, one obtains

$$\begin{aligned} \lambda_L &= \tfrac{1}{5}(C_{11} + 4C_{12} - 2C_{44}),\\ \mu_L &= \tfrac{1}{5}(C_{11} - C_{12} + 3C_{44}),\\ E_1 &= \tfrac{1}{35}C_{111} + \tfrac{18}{35}C_{112} + \tfrac{16}{35}C_{123}\\ &\quad -\tfrac{6}{7}C_{144} - \tfrac{12}{35}C_{244} + \tfrac{16}{35}C_{456},\\ E_2 &= \tfrac{1}{35}C_{111} + \tfrac{4}{35}C_{112} - \tfrac{1}{7}C_{123}\\ &\quad +\tfrac{19}{35}C_{144} + \tfrac{2}{35}C_{244} - \tfrac{12}{35}C_{456},\\ E_3 &= \tfrac{1}{35}C_{111} - \tfrac{3}{35}C_{112} + \tfrac{2}{35}C_{123}\\ &\quad -\tfrac{9}{35}C_{144} + \tfrac{9}{35}C_{244} + \tfrac{9}{35}C_{456}, \end{aligned} \tag{60}$$

where the Voigt notation ($11 \to 1, 22 \to 2, 33 \to 3, 12 \to 4, 23 \to 5, 31 \to 6$) is used. The values of C_{ij} and C_{ijk} in the right-hand side of Eq. (60) have been computed from density-functional theory calculations [39]. Using the values listed in Table I, we obtain the values of λ_L, μ_L, E_1, E_2, and E_3. All the parameters are listed in Table II. As mentioned, the contribution from the term proportional to $(\boldsymbol{e}\cdot\boldsymbol{Q})(\boldsymbol{e}'\cdot\boldsymbol{Q}')(\boldsymbol{e}''\cdot\boldsymbol{Q}'')$ in Eq. (21) can be ignored in the elasticity theory approach. Thus, we can set $E_1 = 0$.

TABLE I. The second- and third-order elastic constants of Al [39] in units of GPa.

C_{11}	110.4	C_{12}	54.5	C_{44}	31.3
C_{111}	−1253	C_{112}	−426	C_{123}	153
C_{144}	−12	C_{166}	−493	C_{456}	−21

To determine the magnitude of the deformation potential for the TA phonons, D_{TA}, introduced phenomenologically below Eq. (24), we set $\beta = 1.5$. The use of Eq. (46) yields $\lambda = 0.383$ ($\lambda_{LA} = 0.191$ and $\lambda_{TA} = 0.096$) and $\lambda\langle\omega^2\rangle = 510.0$ meV^2 ($\lambda_{LA}\langle\omega^2\rangle = 404.9$ meV^2 and $\lambda_{TA}\langle\omega^2\rangle = 52.5$ meV^2), which are similar values reported in Al [8,40].

The BOE given by Eqs. (34) and (35) is solved by the fourth-order Runge-Kutta method, setting the time step of 0.2419 fs. In the present model, the Fermi energy is $\varepsilon_F = 11.695$ eV and the Debye energy for the LA phonon is $E_0 = \hbar\Omega_{LA,D} = 65$ meV. Within an electron energy window of $\varepsilon \in [\varepsilon_F - 10E_0, \varepsilon_F + 10E_0]$, 1600 discrete electron energies are considered. On one hand, 80 and 41 discrete phonon energies for the LA and TA modes are considered.

III. RESULTS AND DISCUSSION

Using $f(\varepsilon)$ and $n_\gamma(\omega)$ at t, the excess electron and phonon energies, measured from the total energies in thermal equilibrium, are computed by

$$E_e = 2\int d\varepsilon\varepsilon\mathcal{N}(\varepsilon)[f(\varepsilon) - f_{FD}(\varepsilon, T_0)], \tag{61}$$

$$E_{ph,\gamma} = \int d\omega\hbar\omega\mathcal{D}_\gamma(\omega)[n_\gamma(\omega) - n_{BE}(\omega, T_0)]. \tag{62}$$

The factor of 2 in Eq. (61) comes from the spin degeneracy. In the present study, we set $T_0 = 25$ meV.

It should be noted that the effect of the e-e scattering on the electron thermalization was found to be negligibly small, that is, the t-E_e curves with and without the e-e scattering effect almost overlap. This seems to be different from the results presented in Ref. [17], where the e-e scattering influences the thermalization. The disagreement with their results would be due to different approximations used for the evaluation of the collision integral: The six-dimensional integral in Eq. (28) is reduced to a three-dimensional [see Eq. (34)] and two-dimensional integral in the present study and Ref. [17], respectively. It should be noted that within the present model the magnitude of the Coulomb pseudopotential μ_C defined in Refs. [16,18] was estimated to be about 0.33, which is a reasonable value in realistic materials. To better understand the thermalization in realistic metals, the use of the wave-vector-dependent coupling functions is desirable, but such a study is out of the scope of this paper.

TABLE II. Material parameters. λ_L, μ_L, E_1, E_2, and E_3 are in units of GPa.

r_s	2.07				
λ_L	53.16	μ_L	29.96		
E_1	−15.23	E_2	−133.83	E_3	−119.63

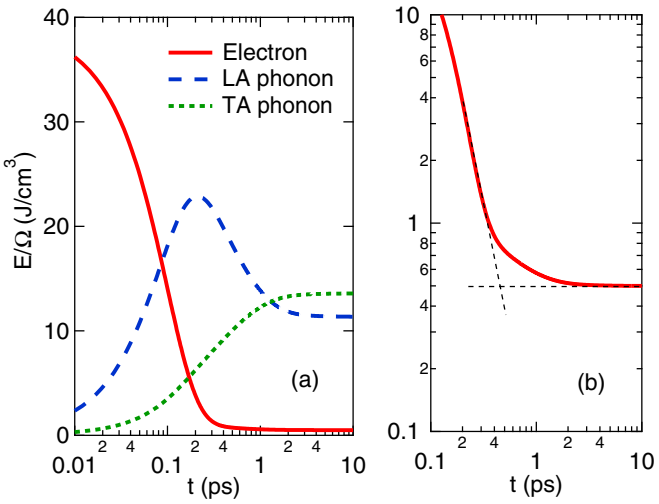

FIG. 1. (a) The t dependence of E_e, $E_{ph,LA}$, and $E_{ph,TA}$($=E_{ph,TA1}=E_{ph,TA2}$) computed by Eqs. (61) and (62). (b) The magnified view of t-E_e curve below $E_e/\Omega = 10$ J/cm^3 in a log-log plot.

A. Thermalization

As a model study, we start from the initial electron distribution function with Gaussian-type peaks above and below the Fermi level, which is given by

$$f(\varepsilon) = f_{FD}(\varepsilon, T_0) + \sum_{s=\pm} s A_s \exp\left[-\left(\frac{\varepsilon - s\varepsilon_0}{2W_e}\right)^2\right], \quad (63)$$

where ε_0 and W_e are the peak position and the width, respectively. Given a peak height A_-, A_+ is uniquely determined by the electron number conservation law. We confirmed that the form of Eq. (63) is similar to laser-excited electron distributions around the Fermi energy described in Refs. [15,17], where the electron-photon scattering processes have been considered explicitly. In addition, similar types of the model functions have been used to study the thermalization in metals [12]. In this subsection, we set $A_- = 0.1$, $\varepsilon_0 = 300$ meV, and $W_e = 50$ meV, where the effective electron temperature amounts to approximately 800 K. The initial phonon distribution is assumed to be $n_{BE}(\omega, T_0)$. In Sec. III B, the effect of the initial electron and phonon distributions on the thermalization will be investigated.

Figure 1(a) shows the t evolution of E_e, $E_{ph,LA}$, and $E_{ph,TA1}$ defined as Eqs. (61) and (62). Since the contribution from $E_{ph,TA2}$ is the same as $E_{ph,TA1}$, the former is not shown in Fig. 1(a). Hereafter, we denote $E_{ph,TA1}$ and $E_{ph,TA2}$ as $E_{ph,TA}$. In the initial stage of the relaxation, $t \leqslant 0.2$ ps, E_e decreases drastically, while $E_{ph,LA}$ and $E_{ph,TA}$ gradually increases. Most of the electron energy is transferred into the LA phonons, resulting in the overshoot of $E_{ph,LA}$ at $t = \tau_0 = 0.21$ ps, followed by a slow decay of $E_{ph,LA}$ and a slow increase in the $E_{ph,TA}$. After $t = 3$ ps, the values of E_{el}, $E_{ph,LA}$, and $E_{ph,TA}$ are almost constant, indicating the thermal equilibrium of the system.

To understand the overshoot of the LA phonon energy, we decompose the energy transfer rate $\partial E_{ph,\gamma}/\partial t$ into a sum of the contribution from the ph-e and ph-ph scattering, which is

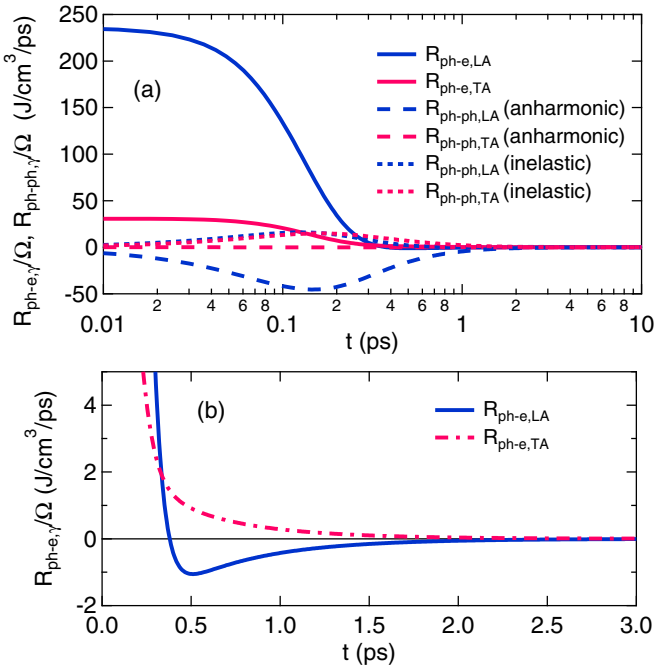

FIG. 2. (a) The t dependence of $R_{ph-e,\gamma}$ and $R_{ph-ph,\gamma}$ with $\gamma =$ LA and TA1 computed from Eqs. (64) and (65). For the inelastic scattering, the curves of $R_{ph-ph,LA}$ and $R_{ph-ph,TA}$ almost overlap. (b) The magnified view of $R_{ph-e,\gamma}$ up to $t = 3$ ps.

defined as, respectively,

$$R_{ph-e,\gamma} = \left(\frac{\partial E_{ph,\gamma}}{\partial t}\right)_{ph-e}, \quad (64)$$

$$R_{ph-ph,\gamma} = \left(\frac{\partial E_{ph,\gamma}}{\partial t}\right)_{ph-ph}. \quad (65)$$

The latter, Eq. (65), is further decomposed into two contributions: the anharmonic decay $R_{ph-ph,\gamma}$(anharmonic) and the inelastic scattering $R_{ph-ph,\gamma}$(inelastic). Similarly, we can define the energy transfer rate of the electronic system due to the e-ph scattering, but the quantity is exactly equal to $-R_{ph-e,\gamma}$.

Figure 2(a) shows $R_{ph-e,\gamma}$ and $R_{ph-ph,\gamma}$ as a function of t. Within the initial relaxation ($t \ll \tau_0$ ps), $R_{ph-e,LA}$ is positive and much larger than the other rates, indicating that the LA phonons obtain a large amount of the electron energy via the ph-e scattering. Simultaneously, the magnitude of $|R_{ph-ph,LA}(\text{anharmonic})|$ increases with increasing t. A negative value of $R_{ph-ph,LA}$(anharmonic) indicates that the LA phonon decays into low-frequency LA and TA phonons. Correspondingly, both of $R_{ph-ph,LA}$(inelastic) $R_{ph-ph,TA}$(inelastic) increase with time. The sum of the contribution from the anharmonic and the inelastic processes, $|R_{ph-ph,LA}|$, becomes larger than the value of $R_{ph-e,LA}$ after $t = \tau_0$ ps. In this way, the overshoot of $E_{ph,LA}$, shown in Fig. 1(a), is due to a crossover from the energy gain via the ph-e scattering to the energy loss via the anharmonic decay into TA phonons.

Figure 1(b) is a magnified view of E_e shown in Fig. 1(a). Before $t \simeq 0.4$ ps, E_e decreases linearly in a log-log plot, while before reaching the thermal equilibrium ($t = 3$ ps) the relaxation behavior slows. Figure 2(b) also shows a magnified

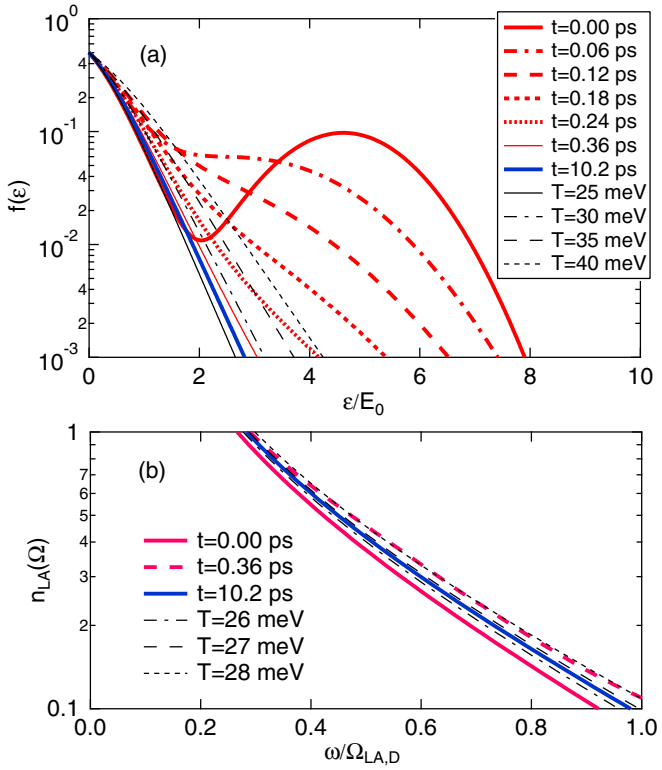

FIG. 3. (a) $f(\varepsilon)$ and (b) $n_{\mathrm{LA}}(\omega)$ for various ts. The FD and BE functions with several Ts are also shown. $f(\varepsilon)$ is nearly an odd function with respect to $\varepsilon = 0$.

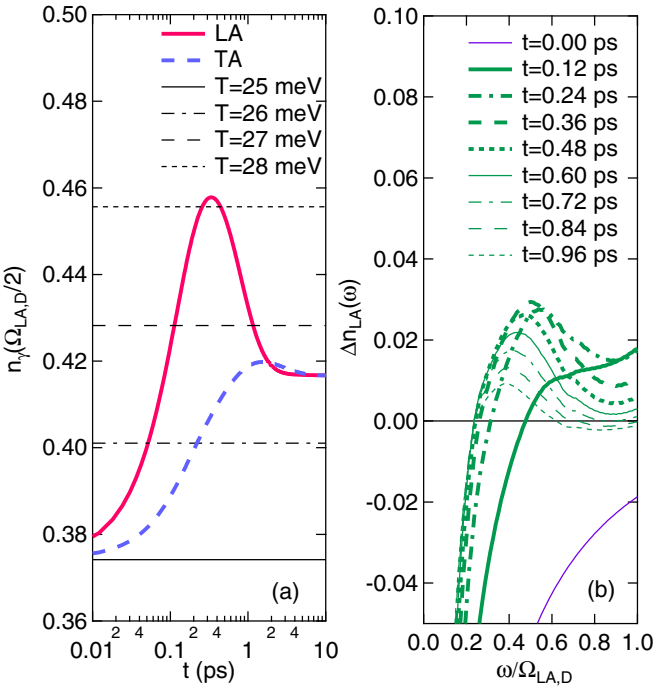

FIG. 4. (a) $n_{\mathrm{LA}}(\Omega_{\mathrm{LA,D}}/2)$ and $n_{\mathrm{TA}}(\Omega_{\mathrm{LA,D}}/2)$ as a function of t. The values of $n_{\mathrm{BE}}(\Omega_{\mathrm{LA,D}}/2, T)$ for $T = 25, 26, 27, 28$ meV are shown. (b) The deviation of $n_{\mathrm{LA}}(\omega)$ from the BE function with $T = 27$ meV for several ts.

view of $R_{\mathrm{ph-e,LA}}$ and $R_{\mathrm{ph-e,TA}}$ in Fig. 1(b). Negative value of $R_{\mathrm{ph-e,LA}}$ is observed during the time interval $t \in [0.38, 4.7]$ ps. This means that the energy stored in the LA phonons is transferred, in turn, into the electronic system. The time interval showing $R_{\mathrm{ph-e,LA}} < 0$ is almost the same as the interval when the electron relaxation slows [Fig. 1(b)]. Thus the appearance of the backward energy flow is an indicator for reaching a thermal equilibrium. A similar scenario involving the backward energy flow has been reported in phononic systems [21]. Note that the negative $R_{\mathrm{ph-e,LA}}$ is also observed after $t = 8.7$ ps, while the value is quite small: $R_{\mathrm{ph-e,LA}} \sim -10^{-4}$ J/(cm^3 ps). This is similar to the dynamics of the damped oscillators in the classical mechanics when $R_{\mathrm{ph-e,LA}}$ in Eq. (64) is regarded as the amplitude of the oscillation.

The decay process discussed above could be understood in terms of the nonequilibrium distribution functions. Figures 3(a) and 3(b) show $f(\varepsilon)$ and $n_{\mathrm{LA}}(\omega)$ for various ts, computed by Eqs. (34) and (35), respectively. For comparison, the FD and BE distribution functions with several Ts are also shown. The Gaussian peak observed at $\varepsilon/E_0 = 5$ in $f(\varepsilon)$ is immediately smeared out within 0.2 ps, while the deviation from the FD function is still not negligible, which is similar to the numerical results in Ref. [18]. After $t = 0.36$ ps, the quasiequilibrium treatment for $f(\varepsilon)$ may be valid, shown in Fig. 3(a). In contrast, the LA phonon population increases due to the ph-e scattering up to $t = 0.36$ ps, after which it decreases, as shown in Fig. 3(b). To understand the phonon dynamics quantitatively, we show the t dependence of $n_\gamma(\omega)$ at $\omega = \Omega_{\mathrm{LA,D}}/2$ in Fig. 4(a). Quite similarly to the t-$E_{\mathrm{ph,LA}}$ curve in Fig. 1(a), an overshoot of the LA phonon population is observed around $t = 0.34$ ps, while the change in $n_{\mathrm{TA}}(\Omega_{\mathrm{LA,D}}/2)$ is moderate. Figure 4(b) shows the deviation of $n_{\mathrm{LA}}(\omega)$ from the BE statistics at $T = 27$ meV for several ts. The phonon population at $\omega = \Omega_{\mathrm{LA,D}}$ increases with time and is maximum at $t = 0.12$ ps, after which it decreases. Since the ph-ph scattering such as LA $\leftrightarrows$ LA + TA frequently occur after the creation of the hot high-frequency LA phonon, the population of the LA phonon with lower frequency ($\omega \simeq \Omega_{\mathrm{LA,D}}/2$) increases with time.

B. Impact of the nonequilibrium distribution

The total energy dynamics within the 4TM and 2TM, described in Secs. II B 4 and II B 5, respectively, are shown in Figs. 5(a). The t-E_{e}, $E_{\mathrm{ph,LA}}$, and $E_{\mathrm{ph,TA}}$ curves in the NEP model are also shown. Clearly, the initial electron relaxation derived from the 2TM and 4TM is faster than that derived from the NEP model. Figure 5(b) shows the relaxation dynamics in the NE+3T and NP+1T models described in Secs. II B 2 and II B 3, respectively. The former model reproduces the initial relaxation in the NEP model, while the latter model improves the relaxation behavior slightly, compared with the 2TM. What is important in these comparative studies is that the energy relaxation in the quasiequilibrium treatment is faster than that in the nonequilibrium treatment. This would lead to an underestimation of the e-ph coupling constant when the 2TM or 4TM are applied to time-resolved experiments. This result, the underestimation of $\lambda\langle\omega^2\rangle$, is consistent with the results reported in Ref. [20].

Finally, we study how the energy relaxation dynamics is changed in response to the initial distribution functions. To

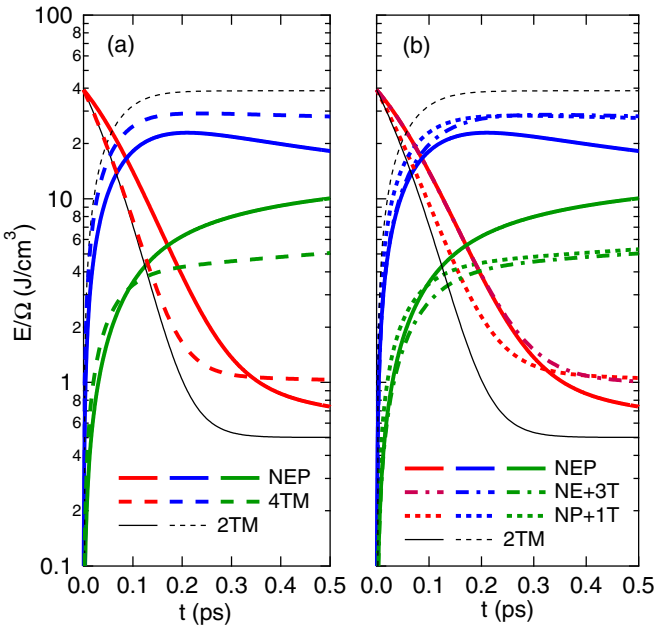

FIG. 5. The t dependence of the excess energies of the electrons (red) and phonons (blue for LA and green for TA) computed within (a) the NEP model, 4TM, and 2TM and (b) the NEP, NE+3T, and NP+1T models, and 2TM. The deviations from the NEP model in E_e for $t > 0.3$ ps and $E_{ph,\gamma}$ for $t > 0.1$ ps are due to the lack of the ph-ph scattering effect in the NE+3T and NP+1T models.

characterize it, we define τ_0, at which $E_{ph,LA}$ is the maximum, as the initial relaxation time, which may be determined from time-resolved diffraction experiments [41,42]. In Eq. (63), we tune three parameters: (i) A_-, (ii) ε_0, and (iii) W_e. We also studied the case of (iv) $f(\varepsilon,t=0)$ equal to the quasiequilibrium distribution with $T_e(t=0)$ higher than T_0. Table III lists the tuned parameters, which determines the magnitude of the excess electron energy given in Eq. (61) at $t=0$. Figure 6 shows τ_0 as a function of $E_e(t=0)$ for various $f(\varepsilon,t=0)$. As expected, τ_0 increases with increasing $E_e(t=0)$ for all cases (i)–(iv). However, the curves of τ_0-$E_e(t=0)$ cannot be described by a single function, implying that τ_0 is *a functional* of $f(\varepsilon,t=0)$. Unfortunately, we could not find a clear relationship between them, whose derivation or microscopic understanding will be a future work. As shown in Fig. 6, the quasiequilibrium approximation, the case (iv), gives the lowest value of τ_0 with E_e fixed. A similar result has been reported in Ref. [15], while the initial distribution used is different from that used in the present study.

More realistically, the electron distribution will change due to the electron-photon interaction within a pulse width [15,17].

TABLE III. Tuned parameters for determining the initial electron distribution function from case (i) to case (iv). ε_0, W_e, and $k_B T_e$ are in units of meV.

(i)	$A_- \in [0.02,0.2]$	$\varepsilon_0 = 300$	$W_e = 50$
(ii)	$A_- = 0.1$	$\varepsilon_0 \in [100,450]$	$W_e = 50$
(iii)	$A_- = 0.1$	$\varepsilon_0 = 300$	$W_e \in [10,100]$
(iv)	$k_B T_e(t=0) \in [30,100]$		

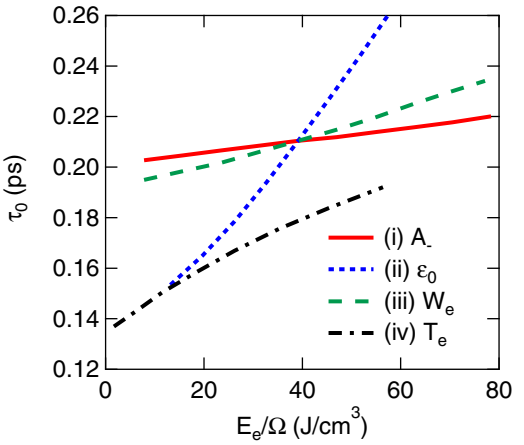

FIG. 6. τ_0 as a function of $E_e(t=0)$ for various initial conditions, $f(\varepsilon,t=0)$s, from case (i) to case (iv) listed in Table III. The initial phonon distribution function is assumed to be the BE function with T_0.

During the finite pulse width, the phonons are also created through the ph-e scattering, disturbing the phonon distribution function. To consider this effect, we assume that the initial LA phonon distribution is given as

$$n_{LA}(\omega) = n_{BE}(\omega,T_0) + B\exp\left[-\left(\frac{\omega-\Omega_{LA,D}}{2W_{ph}/\hbar}\right)^2\right], \quad (66)$$

where B and W_{ph} are the peak height and the width. We also consider the case that the initial distribution is equal to the quasiequilibrium distribution $n_{LA}(\omega) = n_{BE}(\omega,T_{ph})$ with $T_{ph} \geqslant T_0$. $n_{TA}(\omega)$ is assumed to be equal to $n_{BE}(\omega,T_0)$ at $t=0$ ps because the magnitude of the electron-TA phonon coupling is smaller than that of the electron-LA phonon coupling. The initial electron distribution is still expressed as Eq. (63), where $A_- = 0.1$, $\varepsilon_0 = 300$ meV, and $W_e = 50$ meV, yielding $E_e(t=0)/\Omega \simeq 40$ J/cm^3. Table IV lists the tuned parameters for the initial phonon distribution function: From case (v) to case (vii). Positive B or $T_{ph} - T_0$ yields a positive value of $E_{ph}(t=0)$. Figure 7 shows τ_0 as a function of $E_e(t=0) + E_{ph}(t=0)$. Contrary to the cases of (i)–(iv), τ_0 decreases as the sum of the excess energies increases. This means that the anharmonic decay event occurs frequently with increasing $E_{ph,LA}(t=0)$, as a result of which τ_0 becomes shorter. The overshoot of $E_{ph,LA}$ will thus vanish if $E_{ph,LA}(t=0)/E_e(t=0) \gg 1$. Based on this scenario, it is easy to understand the result of the case (vii): The quasiequilibrium distribution approximation gives the highest value of τ_0 with $E_e + E_{ph}$ fixed, since the anharmonic decay rate slows. What is suggested by these special conditions is

TABLE IV. Tuned parameters for determining the initial phonon distribution function from case (v) to case (vii). W_{ph} and $k_B T_{ph}$ are in units of meV.

(v)	$B \in [0,0.16]$	$W_{ph} = 50$
(vi)	$B = 0.1$	$W_{ph} \in [0.02,0.20]$
(vii)	$k_B T_{ph}(t=0) \in [25,35]$	

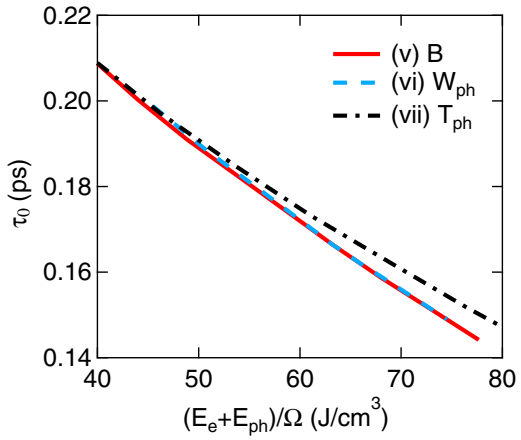

FIG. 7. τ_0 as a function of $E_e(t=0)+E_{ph}(t=0)$ for various $n_{LA}(\omega,t=0)$s from case (v) to case (vii) listed in Table IV. The parameters for the initial electron distribution are set to be $A_-=0.1$, $\varepsilon_0=300$ meV, and $W_e=50$ meV, which yields $E_e(t=0)/\Omega\simeq 40$ J/cm^3. The plotted curves for (v) and (vi) almost overlap.

that the anharmonic phonon decay would play an important role in understanding the thermalization in metals.

IV. SUMMARY

We have studied the electron and phonon thermalization in photoexcited metals by solving the BOE taking into account the e-e, e-ph, ph-e, and ph-ph scattering. We have found that in the initial stage of the relaxation, most of the electron energy is transferred into the LA phonons through the e-ph and ph-e scattering. Simultaneously, the LA phonon decays into TA phonons via the ph-ph scattering. This yields an overshoot of the total LA phonon energy at a time τ_0. The behavior of the thermalization is not affected by the presence of the e-e scattering. The picture for the thermalization demonstrated in the present study is quite different from the 2TM scenario [3].

By systematically investigating the relaxation dynamics of several models, we have shown that the energy relaxation within the quasiequilibrium approximation is found to be faster than that in a realistic situation. This implies that the use of the 2TM underestimates the e-ph coupling constant in metals, consistent with the results in Ref. [20].

We have also found that the relaxation time τ_0 strongly depends on the initial distribution functions $f(\varepsilon,t=0)$ and $n_\gamma(\omega,t=0)$ as well as the initial energy. An open question is to find a functional form to estimate τ_0. Such a functional must also contain the information about the e-ph and ph-ph interactions.

ACKNOWLEDGMENT

This study is supported by a Grant-in-Aid for Young Scientists B (Grant No. 15K17435) from JSPS.

APPENDIX: DETAILS OF THE COUPLING FUNCTIONS

We first outline the derivation of Eq. (40) from Eq. (36). Due to the spherical symmetry, it is reasonable to express the summation in Eq. (40) by

$$\sum_{\boldsymbol{k}}\to\frac{\Omega}{(2\pi)^3}\int_0^\infty dk k^2\int_0^\pi d\theta_{\boldsymbol{k}}\sin\theta_{\boldsymbol{k}}\int_0^{2\pi}d\phi_{\boldsymbol{k}}. \quad \text{(A1)}$$

Similarly, the summations with respect to $\boldsymbol{k}'$ and $\boldsymbol{q}$ are transformed into the integrals. Without loss of generality, we consider that $\boldsymbol{q}$ is parallel to the z axis. Then, $\theta_{\boldsymbol{k}}$, $\phi_{\boldsymbol{k}}$, $\theta_{\boldsymbol{q}}$, and $\phi_{\boldsymbol{q}}$ can be regarded as the relative angle for $\boldsymbol{q}$. Then, one obtains

$$C_{e-e}(\varepsilon,\varepsilon';\xi,\xi')=\frac{4\pi^3}{\hbar\mathcal{N}(\varepsilon)}\left(\frac{2m^2}{\hbar^4}\right)^2\int_0^\pi d\theta_{\boldsymbol{k}}\int_0^\pi d\theta_{\boldsymbol{k}'}\times\int_0^\infty dq|\tilde{V}(\boldsymbol{q})|^2\delta\left(\theta_{\boldsymbol{k}}-\theta_{\boldsymbol{k}}^0\right)\delta\left(\theta_{\boldsymbol{k}'}-\theta_{\boldsymbol{k}'}^0\right), \quad \text{(A2)}$$

where $\theta_{\boldsymbol{k}}^0$ and $\theta_{\boldsymbol{k}'}^0$ are given by

$$\theta_{\boldsymbol{k}}^0=\arccos\left[\frac{\sqrt{2m}}{2\hbar q\sqrt{\varepsilon}}(\xi-\varepsilon-\varepsilon_{\boldsymbol{q}})\right],$$
$$\theta_{\boldsymbol{k}'}^0=\arccos\left[-\frac{\sqrt{2m}}{2\hbar q\sqrt{\varepsilon'}}(\xi'-\varepsilon'-\varepsilon_{\boldsymbol{q}})\right], \quad \text{(A3)}$$

respectively. If $0\leqslant\theta_{\boldsymbol{k}}^0\leqslant\pi$ and $0\leqslant\theta_{\boldsymbol{k}'}^0\leqslant\pi$, the integration with respect to $\theta_{\boldsymbol{k}}$ and $\theta_{\boldsymbol{k}'}$ becomes unity. Thus, one obtains Eq. (40) in the main text. It would be straightforward to derive Eq. (41) from Eq. (37).

We next consider the numerical implementation of Eq. (39). Using the spherical coordinates, we express the phonon wave vector and the polarization vectors as follows

$$\begin{aligned}\boldsymbol{Q}&=Q\boldsymbol{e}_r,\\ \boldsymbol{e}(\boldsymbol{Q},\mathrm{LA})&=\boldsymbol{e}_r=(\sin\theta\cos\phi,\sin\theta\sin\phi,\cos\theta),\\ \boldsymbol{e}(\boldsymbol{Q},\mathrm{TA1})&=\boldsymbol{e}_\theta=(\cos\theta\cos\phi,\cos\theta\sin\phi,-\sin\theta),\\ \boldsymbol{e}(\boldsymbol{Q},\mathrm{TA2})&=\boldsymbol{e}_\phi=(-\sin\phi,\cos\phi,0),\end{aligned} \quad \text{(A4)}$$

where the abbreviation of $\theta=\theta_{\boldsymbol{Q}}$ and $\phi=\phi_{\boldsymbol{Q}}$ is used. Similarly, we define

$$\begin{aligned}\boldsymbol{Q}'&=Q'\boldsymbol{e}_r',\\ \boldsymbol{e}(\boldsymbol{Q}',\mathrm{LA})&=(\sin\theta'\cos\phi',\sin\theta'\sin\phi',\cos\theta'),\\ \boldsymbol{e}(\boldsymbol{Q}',\mathrm{TA1})&=(\cos\theta'\cos\phi',\cos\theta'\sin\phi',-\sin\theta'),\\ \boldsymbol{e}(\boldsymbol{Q}',\mathrm{TA2})&=(-\sin\phi',\cos\phi',0),\end{aligned} \quad \text{(A5)}$$

where $\theta'=\theta_{\boldsymbol{Q}'}$ and $\phi'=\phi_{\boldsymbol{Q}'}$. Using these expressions, we can obtain the expressions for $\boldsymbol{Q}+\boldsymbol{Q}'$ and $\boldsymbol{e}(\boldsymbol{Q}+\boldsymbol{Q}',\gamma'')$ in terms

of $Q, Q', \theta, \theta', \phi$, and ϕ'. Then one obtains

$$C_{\mathrm{ph-ph}}(\omega,\omega',\omega'',\gamma,\gamma',\gamma'') = \frac{\Omega}{(2\pi)^6 \hbar \mathcal{D}_\gamma(\omega)} \left(\frac{\hbar}{2\rho_i}\right)^3 \int dS \int dS' \times \frac{\omega\omega'}{(v_\gamma v_{\gamma'})^3} \frac{|A_{\mathrm{ph}}|^2}{v_{\gamma''}|\boldsymbol{Q}+\boldsymbol{Q}'|} \delta(\omega'' - v_{\gamma''}|\boldsymbol{Q}+\boldsymbol{Q}'|), \tag{A6}$$

where $\int dS = \int d\theta \sin\theta \int d\phi$. The numerical integrals for θ and ϕ are efficiently performed by using the spherical design [43]. In the present work, 86 points on a sphere were used. The Dirac-delta function in Eq. (A6) is approximated to the Gaussian function with the broadening of $0.02E_0$. To reduce the numerical errors of the total energy, we used the symmetry properties of $f(\omega,\omega',\omega'',\gamma,\gamma',\gamma'') = \mathcal{D}_\gamma(\omega) C_{\mathrm{ph-ph}}(\omega,\omega',\omega'',\gamma,\gamma',\gamma'')$ with the replacement of $(\omega,\gamma) \leftrightarrow (\omega',\gamma') \leftrightarrow (\omega'',\gamma'')$. Using the averaged value of fs, that is,

$$\tfrac{1}{6}[f(\omega,\omega',\omega'',\gamma,\gamma',\gamma'') + f(\omega,\omega'',\omega',\gamma,\gamma'',\gamma') + f(\omega',\omega,\omega'',\gamma',\gamma,\gamma'') + f(\omega',\omega'',\omega,\gamma',\gamma'',\gamma) + f(\omega'',\omega,\omega',\gamma'',\gamma,\gamma') + f(\omega'',\omega',\omega,\gamma'',\gamma',\gamma)],$$

we redefine the ph-ph coupling function as $C_{\mathrm{ph-ph}}(\omega,\omega',\omega'',\gamma,\gamma',\gamma'') = f(\omega,\omega',\omega'',\gamma,\gamma',\gamma'')/\mathcal{D}_\gamma(\omega)$.

[1] M. I. Kaganov, I. M. Lifshitz, and L. V. Tanatarov, Relation between Electrons and the Crystalline Lattice, Zh. Eksp. Teor. Fiz. **31**, 232 (1956) [Sov. Phys. JETP **4**, 173 (1957)].

[2] S. I. Anisimov, B. L. Kapeliovich, and T. L. Perel'man, Electron emission from metal surfaces exposed to ultrashort laser pulses, Zh. Eksp. Teor. Fiz. **66**, 776 (1974) [Sov. Phys. JETP **39**, 375 (1974)].

[3] P. B. Allen, Theory of Thermal Relaxation of Electrons in Metals, Phys. Rev. Lett. **59**, 1460 (1987).

[4] S. D. Brorson, A. Kazeroonian, J. S. Moodera, D. W. Face, T. K. Cheng, E. P. Ippen, M. S. Dresselhaus, and G. Dresselhaus, Femtosecond Room-Temperature Measurement of the Electron-Phonon Coupling Constant λ in Metallic Superconductors, Phys. Rev. Lett. **64**, 2172 (1990).

[5] L. Perfetti, P. A. Loukakos, M. Lisowski, U. Bovensiepen, H. Eisaki, and M. Wolf, Ultrafast Electron Relaxation in Superconducting $Bi_2Sr_2CaCu_2O_8 + \delta$ by Time-Resolved Photoelectron Spectroscopy, Phys. Rev. Lett. **99**, 197001 (2007).

[6] Y. C. Tian, W. H. Zhang, F. S. Li, Y. L. Wu, Q. Wu, F. Sun, G. Y. Zhou, L. Wang, X. Ma, Q.-K. Xue, and J. Zhao, Ultrafast Dynamics Evidence of High Temperature Superconductivity in Single Unit Cell FeSe on $SrTiO_3$, Phys. Rev. Lett. **116**, 107001 (2016).

[7] A. Sterzi, A. Crepaldi, F. Cilento, G. Manzoni, E. Frantzeskakis, M. Zacchigna, E. van Heumen, Y. K. Huang, M. S. Golden, and F. Parmigiani, SmB_6 electron-phonon coupling constant from time- and angle-resolved photoelectron spectroscopy, Phys. Rev. B **94**, 081111(R) (2016).

[8] Z. Lin, L. V. Zhigilei, and V. Celli, Electron-phonon coupling and electron heat capacity of metals under conditions of strong electron-phonon nonequilibrium, Phys. Rev. B **77**, 075133 (2008).

[9] R. Lundgren and G. A. Fiete, Electronic cooling in Weyl and Dirac semimetals, Phys. Rev. B **92**, 125139 (2015).

[10] A. M. Brown, R. Sundararaman, P. Narang, W. A. Goddard III, and H. A. Atwater, Ab initio phonon coupling and optical response of hot electrons in plasmonic metals, Phys. Rev. B **94**, 075120 (2016).

[11] W. S. Fann, R. Storz, H. W. K. Tom, and J. Bokor, Electron thermalization in gold, Phys. Rev. B **46**, 13592 (1992).

[12] R. H. M. Groeneveld, R. Sprik, and Ad. Lagendijk, Femtosecond spectroscopy of electron-electron and electron-phonon energy relaxation in Ag and Au, Phys. Rev. B **51**, 11433 (1995).

[13] M. Lisowski, P. A. Loukakos, U. Bovensiepen, J. Stahler, C. Gahl, and M. Wolf, Ultra-fast dynamics of electron thermalization, cooling and transport effects in Ru(001), Appl. Phys. A **78**, 165 (2004).

[14] Y. Ishida, T. Togashi, K. Yamamoto, M. Tanaka, T. Taniuchi, T. Kiss, M. Nakajima, T. Suemoto, and S. Shin, Non-thermal hot electrons ultrafastly generating hot optical phonons in graphite, Sci. Rep. **1**, 64 (2011).

[15] B. Rethfeld, A. Kaiser, M. Vicanek, and G. Simon, Ultrafast dynamics of nonequilibrium electrons in metals under femtosecond laser irradiation, Phys. Rev. B **65**, 214303 (2002).

[16] V. V. Kabanov and A. S. Alexandrov, Electron relaxation in metals: Theory and exact analytical solutions, Phys. Rev. B **78**, 174514 (2008).

[17] B. Y. Mueller and B. Rethfeld, Relaxation dynamics in laser-excited metals under nonequilibrium conditions, Phys. Rev. B **87**, 035139 (2013).

[18] V. V. Baranov and V. V. Kabanov, Theory of electronic relaxation in a metal excited by an ultrafast optical pump, Phys. Rev. B **89**, 125102 (2014).

[19] A. F. Kemper, O. Abdurazakov, and J. K. Freericks, arXiv:1708.05725.

[20] L. Waldecker, R. Bertoni, and R. Ernstorfer, and J. Vorberger, Electron-Phonon Coupling and Energy Flow in a Simple Metal beyond the Two-Temperature Approximation, Phys. Rev. X **6**, 021003 (2016).

[21] S. Ono, Nonequilibrium phonon dynamics beyond the quasiequilibrium approach, Phys. Rev. B **96**, 024301 (2017).

[22] P. Maldonado, K. Carva, M. Flammer, and P. M. Oppeneer, Theory of Out-of-Equilibrium Ultrafast Relaxation Dynamics in Metals, Phys. Rev. B **96**, 174439 (2017).

[23] I. Klett and B. Rethfeld, arXiv:1710.02355.

[24] S. Sadasivam, M. K. Y. Chan, and P. Darancet, Theory of Thermal Relaxation of Electrons in Semiconductors, Phys. Rev. Lett. **119**, 136602 (2017).

[25] Y. Ishida, H. Masuda, H. Sakai, S. Ishiwata, and S. Shin, Revealing the ultrafast light-to-matter energy conversion before heat diffusion in a layered Dirac semimetal, Phys. Rev. B **93**, 100302(R) (2016).

[26] C. Gadermaier, A. S. Alexandrov, V. V. Kabanov, P. Kusar, T. Mertelj, X. Yao, C. Manzoni, D. Brida, G. Cerullo, and D. Mihailovic, Electron-Phonon Coupling in High-Temperature

Cuprate Superconductors Determined from Electron Relaxation Rates, Phys. Rev. Lett. **105**, 257001 (2010).

[27] C. Gadermaier, V. V. Kabanov, A. S. Alexandrov, L. Stojchevska, T. Mertelj, C. Manzoni, G. Cerullo, N. D. Zhigadlo, J. Karpinski, Y. Q. Cai, X. Yao, Y. Toda, M. Oda, S. Sugai, and D. Mihailovic, Strain-Induced Enhancement of the Electron Energy Relaxation in Strongly Correlated Superconductors, Phys. Rev. X **4**, 011056 (2014).

[28] S. Ono, Y. Toda, and J. Onoe, Unified understanding of the electron-phonon coupling strength for nanocarbon allotropes, Phys. Rev. B **90**, 155435 (2014).

[29] Y. Murakami, P. Werner, N. Tsuji, and H. Aoki, Interaction quench in the Holstein model: Thermalization crossover from electron- to phonon-dominated relaxation, Phys. Rev. B **91**, 045128 (2015).

[30] F. Dorfner, L. Vidmar, C. Brockt, E. Jeckelmann, and F. Heidrich-Meisner, Real-time decay of a highly excited charge carrier in the one-dimensional Holstein model, Phys. Rev. B **91**, 104302 (2015).

[31] J. Kogoj, L. Vidmar, M. Mierzejewski, S. A. Trugman, and J. Bonča, Thermalization after photoexcitation from the perspective of optical spectroscopy, Phys. Rev. B **94**, 014304 (2016).

[32] N. W. Ashcroft, N. D. Mermin, and D. Wei, *Solid State Physics*, revised edition (Cengage Learning, Singapore, 2016).

[33] A. L. Fetter and J. D. Walecka, *Quantum Theory of Many-Particle Systems* (Dover, New York, 2003).

[34] A. A. Maradudin, *Dynamical Properties of Solids*, edited by G. K. Horton and A. A. Maradudin (North-Holland, Amsterdam, 1974).

[35] J. M. Ziman, *Electrons and Phonons* (Oxford University Press, New York, 1960).

[36] L. D. Landau and E. M. Lifshitz, *Physical Kinetics* (Pergamon Press, Oxford, 1981).

[37] S. Tamura, Spontaneous decay rates of LA phonons in quasi-isotropic solids, Phys. Rev. B **31**, 2574(R) (1985).

[38] H. Smith and H. H. Jensen, *Transport Phenomena* (Oxford University Press, New York, 1989).

[39] H. Wang and M. Li, Ab initio calculations of second-, third-, and fourth-order elastic constants for single crystals, Phys. Rev. B **79**, 224102 (2009).

[40] G. Grimvall, *The Electron-Phonon Interaction in Metals* (North-Holland, Amsterdam, 1981).

[41] M. Trigo, J. Chen, V. H. Vishwanath, Y. M. Sheu, T. Graber, R. Henning, and D. A. Reis, Imaging nonequilibrium atomic vibrations with x-ray diffuse scattering, Phys. Rev. B **82**, 235205 (2010).

[42] M. Harb, H. Enquist, A. Jurgilaitis, F. T. Tuyakova, A. N. Obraztsov, and J. Larsson, Phonon-phonon interactions in photoexcited graphite studied by ultrafast electron diffraction, Phys. Rev. B **93**, 104104 (2016).

[43] http://web.maths.unsw.edu.au/~rsw/Sphere/EffSphDes/.